A Level-Set Corrector to an Adaptive Multiscale Permeability Prediction

Inga Berre (inga.berre@mi.uib.no)
Department of Mathematics, University of Bergen, Johs. Brunsgt. 12, N-5008 Bergen, Norway and
CIPR-Centre for Integrated Petroleum Research, University of Bergen, Realfagbygget, Allégaten 41, N-5007 Bergen, Norway

Martha Lien (martha.lien@cipr.uib.no)
CIPR-Centre for Integrated Petroleum Research, University of Bergen, Realfagbygget, Allégaten 41, N-5007 Bergen, Norway and
Department of Mathematics, University of Bergen, Johs. Brunsgt. 12, N-5008 Bergen, Norway

Trond Mannseth (trond.mannseth@cipr.uib.no)
CIPR-Centre for Integrated Petroleum Research, University of Bergen, Realfagbygget, Allégaten 41, N-5007 Bergen, Norway and
Department of Mathematics, University of Bergen, Johs. Brunsgt. 12, N-5008 Bergen, Norway

Abstract. We consider the inverse problem of permeability estimation for two-phase porous-media flow. The novel approach is based on regularization by zonation, where the geometry and size of the regions are chosen adaptively during the optimization procedure. To achieve this, we have utilized level-set functions to represent the permeability.

The available data are sparsely distributed in space; hence, it is reasonable to confine the estimation to coarse-scale structures. The level-set approach is able to alter the boundaries between regions of different permeability without strict restrictions on their shape; however, when the data are sparse, a reasonable initial guess for the permeability is required. For this task, we use adaptive multiscale permeability estimation, which has the potential of identifying main permeability variations. These are described by a piecewise constant function, where the constant values are attained on rectangular zones.

In the current work, we develop a level-set corrector strategy, assuming adaptive multiscale permeability estimation as a predictor.

Keywords: inverse problem, permeability estimation, two-phase flow, regularization, level-set representation, adaptive multiscale estimation

1. Introduction

History matching of production data is important to determine vital physical characteristics of a reservoir. In this paper, we are con-

cerned with the spatial characteristic of absolute permeability, which is required to perform simulations that can predict reservoir behavior.

Information sources for the permeability estimation problem can be static well data, up-scaled geological data, and dynamic well data. In this work, we assume no prior knowledge of permeability structures as from a geological model. The only source of information considered for the estimation procedure is pressure data from wells (dynamic well data).

Our approach to this inverse problem is a *predictor-corrector* strategy. For each estimation problem, we assume that an adaptive multiscale estimation (AME) (Grimstad et al., 2003) has been carried out. Subsequently, using a level-set representation of the permeability, we correct the AME result by allowing for more general geometry of the regions of constant permeability.

The purpose of AME is to find a permeability estimate by solving a sequence of parameter estimation problems with increasing dimension. In the method, the reservoir is partitioned sequentially into rectangular regions of decreasing size. The partitionings are chosen by considering a selection criterion based on the available data, so that a region hopefully is divided only if there is support for this in the data. At convergence the domain consists of rectangular sub-regions of different size. However, because of restrictions on how the regions are partitioned, AME can lead to over-parameterization.

We propose a methodology that can improve the result after a step of AME, progressing the optimization by allowing for more general zone geometry. This is obtained using a level-set representation of the interior boundaries between regions of different constant permeability. The boundaries between the regions can then be deformed to obtain a better zonation, preventing over-parameterization. We denote this strategy as *level-set correction* (LSC) of the permeability.

The level-set idea for representation of moving curves or interfaces was first introduced by Osher and Sethian (1988), and it has several advantages. Topological changes such as splitting or merging of curves do, for instance, cause no difficulties.

In the last decade, level-set methods have been popular for solving inverse problems within imaging (Santosa, 1995/96; Vese and Chan, 2002; Hintermüller, 2003; Burger, 2004). Level-set methods have also been applied for recovering piecewise constant coefficients in elliptic equations (Ito et al., 2001; Heimsund et al., 2003; Chan and Tai, 2003). These inverse problems are, however, characterized by a large spatial density of data. The permeability estimation problem we consider is, in contrast, characterized by a very sparse spatial distribution of data. In addition, our forward problem requires much heavier compu-

tations. Hence, the LSC strategy for permeability estimation is constructed to obtain a permeability estimate with few updates on the level-set functions. This is done by combining a restricted representation of the level-set functions by an optimization algorithm with rapid convergence.

We focus on the potential of the LSC strategy for improving the result after one or more steps of AME by altering the geometry of the zones. Hence, our initial guess for the level-set estimation corresponds to what we could expect if AME had been applied as a predictor.

We start by giving the model equations for porous-media flow in Section 2 before we present the problem of permeability estimation and consider the ill-posedness of this problem in Section 3. A brief description outlining the main ideas of AME is given in Section 4. Next, in Section 5, we introduce a level-set representation of the permeability and propose a strategy for permeability estimation using this representation. Numerical results based on the proposed solution algorithm are presented in Section 6. Some further remarks about how AME and LSC can be combined are made in Section 7 before we conclude in Section 8.

2. Forward Model for Porous-Media Flow

By means of Darcy's law, conservation of mass for two-phase, incompressible, and immiscible porous-media flow in a gravity-free environment with isotropic permeability gives the following equations:

$$\begin{aligned}\varphi(\mathbf{x})\frac{\partial S_o}{\partial t} - \nabla\cdot(k(\mathbf{x})k_{ro}(S_o)\mu_o^{-1}\nabla p_o) &= q_o,\\ \varphi(\mathbf{x})\frac{\partial S_w}{\partial t} - \nabla\cdot(k(\mathbf{x})k_{rw}(S_w)\mu_w^{-1}\nabla p_w) &= q_w.\end{aligned}$$

Here the subscripts refer to the oil phase (o) and water phase (w). Furthermore, with respect to the ith fluid phase, S_i denotes the saturation, which is the volume fraction of fluid in the pores; p_i is the pressure; k_{ri} is the relative permeability; μ_i is the viscosity; and q_i is the external volumetric flow rate. The porosity and the absolute permeability of the medium are denoted by $\varphi(\mathbf{x})$ and $k(\mathbf{x})$, respectively.

The equations are defined for $(x,t) \in \Omega \times [0,T]$, where Ω is a bounded, two-dimensional reservoir domain and T is finite. We assume irreducible water saturation as initial condition and no-flow boundary conditions.

Closure of the system is obtained by assuming that the porous medium is completely saturated, together with an equation of state

defining the capillary pressure:

$$\begin{aligned} S_0 + S_w &= 1, \\ p_o - p_w &= P_c(S_w). \end{aligned}$$

3. Inverse Problem

We are concerned with estimating absolute permeability, $k(\mathbf{x})$, assuming the other model specifications to be known.

As information source, we use dynamic data from wells; more specifically, these include time series of pressures sampled in the injection wells during production. Hence, the permeability estimation problem is an inverse problem. Since drilling a well is expensive, the spatial distribution of the dynamic well data is typically very sparse. Consequently, the problem of estimating permeability in each grid cell of the computational domain is ill-posed, which can result in huge uncertainties in the parameters even if the measurement errors are small.

The original ill-posed problem must be regularized to gain a better posed problem; see, for example the reviews by Yeh (1986), Carrera (1988), Sun (1994), de Marsily et al. (2000), McLaughlin and Townley (1996), and Oliver et al. (2001). The different strategies developed to address this task can be classified into two groups: The strategies compensating for deliberate over-parameterization by penalizing deviations from prior knowledge about the sought solution as given by the geological model; and the strategies applying a reduced parameterization of the sought permeability function. While an example of the former is maximum likelihood estimation (Gavalas et al., 1976) and Tikhonov regularization (e.g., Kirsch, 1996), a typical regularization strategy that fit in the latter category is to reduce the dimension of the parameter space by dividing the reservoir into zones of constant permeability value (Jacquard, 1964; see Jacquard and Jain, 1965). This strategy is referred to as zonation in the literature, and we focus on this type of regularization in the following.

It is a challenge to determine the number and geometry of zones prior to the estimation. A too low resolution can result in data not being reconciled, while a too high resolution can lead to unnecessary computational work and often to estimated permeability values being out of range. The latter problem is usually referred to as over-parameterization. A strategy to avoid over-parameterization is to initially apply a minimum number of zones and successively increase the

dimension of the parameter space by sequential division of zones into sub-zones.

In ordinary multiscale estimation, a regular grid for the zonation is uniformly refined at each estimation step (Emsellem and de Marsily, 1971). This implies that a two-dimensional region is partitioned into four sub-regions. Yoon et al. (1999) applies this method to permeability estimation for two-phase flow given sparsely distributed data.

Ordinary multiscale estimation is further expanded on by introducing adaptivity into the refinement process, so that partitioning of a zone is done only when there is support in the available data for an increased number of parameters. Adaptive multiscale permeability estimation (Grimstad et al., 2003) is an example of this strategy; the number of new parameters at each step depends on the available data. The partitioning of the zones is restricted to rectangular and congruent sub-regions. Although the partitioning in AME is extended by Krüger and Mannseth (2004) to also include triangles, the requirements set on the geometry and size of the zones are still a drawback of this strategy. A related approach to AME is proposed by Ben Ameur at al. (2002). They apply it for estimating hydraulic transmissivities for one-phase flow given a high spatial data density.

3.1. Parameter Estimation Problem

Given a representation of the permeability function

$$k(\mathbf{x}) = k(\mathbf{c}, \{\psi_i(\mathbf{x})\})$$

by means of some basis functions $\{\psi_i(\mathbf{x})\}$, we are able to formulate the parameter estimation problem.

Let $\mathbf{d} \in \mathbb{R}^M$ denote all the values in the time series of measured well pressures. Correspondingly, let $\mathbf{m} \in \mathbb{R}^M$ represent the pressures calculated using the forward model.

The residual can be written as

$$\mathbf{r}(\mathbf{c}) = \mathbf{d} - \mathbf{m}(\mathbf{c}).$$

The parameter estimation problem is now as follows: Find $\mathbf{c}^*$ such that

$$\mathbf{c}^* = \arg\min_{\mathbf{c}} ||\mathbf{r}(\mathbf{c})||$$

for some norm $||\cdot||$ on $\mathbb{R}^M$. The estimation problem is solved by finding the parameter vector that minimizes the residual norm. We apply a weighted least-squares objective function, and, since we focus on the regularizing effect of a reduced parameterization, we do not include a

penalty term based on prior knowledge about the solution. Hence, the objective function is given as

$$f(\mathbf{c}) = \big(\mathbf{d} - \mathbf{m}(\mathbf{c})\big)^T \mathbf{D}^{-1} \big(\mathbf{d} - \mathbf{m}(\mathbf{c})\big). \tag{1}$$

Here $\mathbf{D}$ is the covariance of the measurement errors $\mathbf{d}_\epsilon$, where $\mathbf{d} = \mathbf{d}_{true} + \mathbf{d}_\epsilon$.

3.2. Error in the Estimated Parameters

The errors in the estimated parameters can be separated into two main groups: modeling errors and estimation errors. The estimation errors are a combination of bias and variance errors. Bias errors are caused by the inability of the chosen functional representation to accurately represent the unknown permeability distribution. The variance errors are statistical errors caused by the uncertainty in the measured data. Modeling errors are not considered in the following.

We assume a normal distribution of measurement errors with expected value $E(\mathbf{d}_\epsilon) = 0$ and covariance matrix $\mathbf{D} = \sigma^2\mathbf{I}$, where σ is the standard deviation, and $\mathbf{I}$ is the identity matrix. That is, there are no correlation between succeeding errors.

The estimated parameters $\mathbf{c}^*$ give the lowest possible value of the objective function (1) within the allowed region of parameter space as long as we do not end up in a local minimum. Due to measurement errors, the true permeability may correspond to a larger value of the objective function than the attainable minimum. The randomness in the pressure data implies that the objective function also has a statistical distribution, where the objective-function value given by the reference parameters lies within some interval determined by the specific distribution.

3.3. Solution Criterion

The pressure measurements are in general not equal to the reference pressure. Therefore, there is no basis in the pressure data to minimize the residual further than to some predefined limit depending on the measurement errors. By the assumptions of normally distributed measurement errors and a close to linear objective function (1) near a minimum (Sen and Srivastava, 1990), the objective function is χ^2 distributed with $(M - N)$ number of degrees of freedom:

$$E(f(\mathbf{c}^*)) = M - N,$$

$$\sigma\big(f(\mathbf{c}^*)\big) = \sqrt{2(M - N)}.$$

Here N is the number of parameters for the optimization in question, and M is the total number of pressure observations. We choose as our solution criterion for the inverse problem that the objective function satisfies

$$f(\mathbf{c}) \leq M - N + \sqrt{2(M-N)}. \tag{2}$$

4. Adaptive Multiscale Permeability Estimation

Now we present the main ideas behind AME. For a thorough description we refer to Grimstad et al. (2003). As we do not develop this methodology further, we confine our presentation to a brief outline.

Starting at a permeability estimation problem, the number of parameters required to reconcile the observation data is unknown. The strategy of multiscale permeability estimation is to solve a sequence of parameter estimation problems, hierarchically increasing the number of parameters from an initial choice of one parameter for the whole reservoir. Due to the sparsely distributed data, the multiscale estimation seeks to reproduce coarse-scale permeability structures only. The number of parameters is, hence, expected to be low.

In ordinary multiscale estimation, the resolution is increased by the same amount on the entire grid. In contrast, an important feature of AME is that refinement is sought only in regions where this is supported by the data. The chance of over-parameterization is then reduced; nevertheless, it is not eliminated since there can still be a fast growth in the number of new parameters.

Applying AME, a parameterization of the permeability is obtained by writing

$$k(\mathbf{x}) = \sum_{i=1}^{Z} c_i \psi_i(\mathbf{x}),$$

where $\{\psi_i(\mathbf{x})\}$ denotes a set of piecewise constant basis functions and $\mathbf{c} = (c_1, c_2, \ldots, c_Z) \in \mathbb{R}^Z$ is the parameter vector.

The original AME algorithm divides rectangular sub-regions of the reservoir vertically or horizontally into new rectangular and congruent sub-regions. Which of the valid divisions of the regions that is chosen is based on the *predicted attainable objective-function value* $\tilde{f}$ (Grimstad et al., 2003). This function is an approximation of $\min f(\mathbf{c})$ based on a linearization of $\mathbf{m}(\mathbf{c})$. The best parameterization is then chosen based on comparison of the different $\tilde{f}$ values.

Given the limited set of attainable sub-regions, there are always some permeability distributions easier recoverable than others. Figure 1 shows the optimal refinement process given a reference permeability

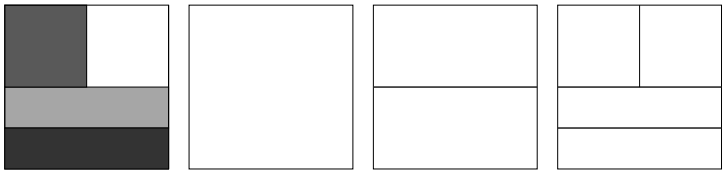

Figure 1. The optimal refinement process required to recover the permeability field in the left plot.

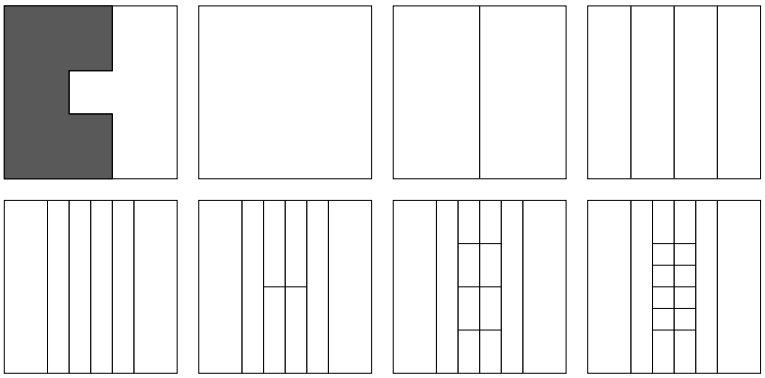

Figure 2. The optimal refinement process required to recover the permeability field in the upper left plot.

with four zones of different constant value. Here the reference permeability can be recovered by four parameters using the AME sub-division strategy.

In the next example, illustrated in Figure 2, the sufficient AME representation consists of 16 parameters even if the reference permeability field takes two constant values only. This is obviously an example of over-parameterization.

After the first AME refinement illustrated in Figure 2, there would be much to gain by deforming the boundary between the sub-regions. This illustrates that allowing for more flexible geometry can significantly reduce the number of zones required to represent the true permeability. Hence, a correction strategy that can alter the geometry of the zones is motivated.

5. Permeability Representation by Level-Set Functions

With AME, there are unfavorable restrictions on the geometry of the zones that can lead to over-parameterization. Since flexible geometry have the potential of describing the reference permeability with a minimum number of zones, the objective of the current work is to improve

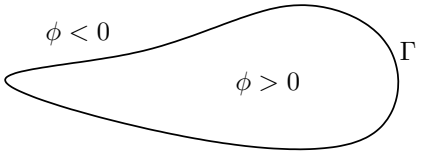

Figure 3. The level-set function.

the permeability estimate from AME by deforming the boundaries between the sub-regions. To achieve this, we utilize level-set functions for the representation of the permeability. In this case, the boundaries between the sub-regions of different constant permeability correspond to the zero isocontours of the level-set functions.

5.1. The Level-Set Idea

The basic elements of implicit representation of a curve or interface by a level-set function are presented here. The idea was first proposed by Osher and Sethian (1988); for a thorough reference, we recommend the book by Osher and Fedkiw (2003). Let Γ be a closed curve in a domain Ω. Alternatively, Γ can be an open curve with endpoints connected to the boundary, $\partial\Omega$. We require ϕ to satisfy:

$$\begin{aligned} \phi(\mathbf{x}) &> 0 \quad \text{if } \mathbf{x} \in \text{interior of } \Gamma; \\ \phi(\mathbf{x}) &< 0 \quad \text{if } \mathbf{x} \in \text{exterior of } \Gamma; \\ \phi(\mathbf{x}) &= 0 \quad \text{for } \mathbf{x} \in \Gamma. \end{aligned} \tag{3}$$

This makes Γ the zero level set of the function ϕ, and ϕ is called the level-set function for Γ; see Figure 3 for a simple illustration. One of the main advantages of the level-set method is that it allows changing topology such as merging and splitting of regions. Traditionally, the level-set function is initialized as the signed distance from the curve Γ.

5.2. Permeability Representation

As the function $k(\mathbf{x})$ may have many different constant values, we need to use multiple level-set functions to represent all regions with different values for the permeability. This is a straightforward follow up of the ideas of Vese and Chan (2002); see also Chan and Tai (2003). Picture for instance three closed curves, Γ_1, Γ_2, and Γ_3. With these curves we associate three level-set functions, ϕ^1, ϕ^2, and ϕ^3. The domain Ω will then be divided into a maximum of eight sub-domains as illustrated in Figure 4. By generalizing, we see that n level-set functions give the

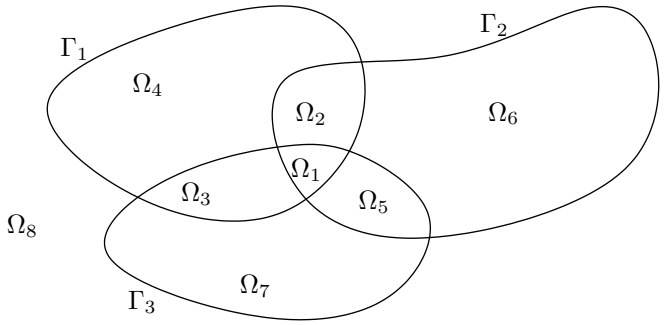

Figure 4. Partition of the domain by the $\phi^l = 0$, $l = 1, \ldots, 3$ iso-contours of the level-set functions.

possibility of 2^n regions. By the definition of the Heaviside function,

$$H(\phi) = \begin{cases} 1, & \text{if } \phi > 0; \\ 0, & \text{if } \phi \leq 0, \end{cases}$$

and the definition of the level-set function (3), we can represent our piecewise constant permeability function as follows:

$$k(\mathbf{x}) = \sum_{i=1}^{2^n} c_i \prod_{j=1}^{n} R_i(\phi^j(\mathbf{x})). \tag{4}$$

Here

$$R_i(\phi^j) = \begin{cases} H(\phi^j), & \text{if } b_i^j = 0; \\ 1 - H(\phi^j), & \text{if } b_i^j = 1, \end{cases}$$

and $\text{bin}(i-1) = (b_i^1, b_i^2, \cdots, b_i^n)$ is the binary representation of $(i-1)$, where $b_i^j = 0$ or 1. Again, considering the example in Figure 4 and applying the formula given in (4), we see that the zonal permeability value in Ω_5, which is inside the curves Γ_2 and Γ_3, but outside the curve Γ_1, is equal to c_5.

Even if we are estimating less than 2^n permeability regions, we can still use n level-set functions since some sub-domains are allowed to be associated with the same constant permeability value. Furthermore, we do not require that the constant values of the coefficients are known a priori as these values can be recovered as a part of our level-set minimization algorithm, which is described in Section 5.6.

5.3. Discretization of the Level-Set Functions

We are solving our equations on a computational grid and, hence, we also need a discrete representation of the level-set functions.

The ill-posedness of the inverse problem of permeability estimation motivates a limited amount of parameters in order to regularize the problem. Also, since we base the optimization procedure on sensitivity calculations that are relatively expensive computationally, a restricted resolution of the representation is beneficial. This is in contrast to previous applications of level-set methods for inverse problems (e.g., Santosa, 1995/96; Vese and Chan, 2002; Hintermüller, 2003; Burger, 2004; Ito et al., 2001; Heimsund et al., 2003; Chan and Tai, 2003), where the resolution of the discretized level-set function corresponds to the underlying computational grid.

To obtain a discrete representation for the level-set functions, we divide the reservoir into N^l elements for each level-set function ϕ^l and write the discretized level-set function as

$$\phi^l(\mathbf{x}) = \sum_{s=1}^{N^l} a_s^l \chi_s^l(\mathbf{x}), \qquad l = 1, \ldots, n.$$

Here $\{\chi_s^l\}$ are characteristic basis functions specifying our representation of ϕ^l, and N^l is the dimension of the parameter space for the representation of ϕ^l. Each parameter a_s^l represents the value of the level-set function for a group of grid cells, so that $N^l \ll (N_x \cdot N_y)$, where N_x and N_y denotes the total number of grid cells in the x- and y-direction, respectively. Letting $\mathbf{a}^l = (a_1^l, a_2^l, \ldots, a_{N^l}^l)$ for $l = 1, \ldots, n$ and $\mathbf{a} = [\mathbf{a}^1\ \mathbf{a}^2\ \ldots\ \mathbf{a}^n]$, we can write

$$k(\mathbf{x}) = k(\mathbf{a}, \{\chi_s^l(\mathbf{x})\}),$$

for fixed values of the permeability coefficient $\mathbf{c}$.

The discretized level-set function, ϕ^l, is initially an approximation to the distance function, where the accuracy depends on the resolution of the discretization.

In the current work, we assume that we have a good initial guess for the permeability based on AME. Therefore, we allow only for sequential, local updates of the boundaries between the zones of different permeability values. Hence, we apply a more detailed representation of the level-set function only in the region close to the zero isocontour. The values of the level-set function outside this region are not allowed to change. This approach is related to the local or narrow band level-set method (Adalsteinsson and Sethian, 1995; Peng et al., 1999). In the narrow band, we apply mostly a coarse representation of the level-set

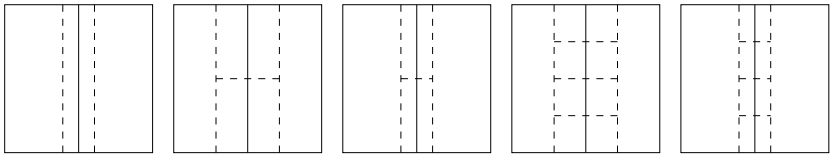

Figure 5. Example of discretizations $P_1, P_2, \ldots, P_5$ (from left to right) for a level-set function. The solid line denotes the zero level set in the figures, whereas the dashed lines illustrate the discretization.

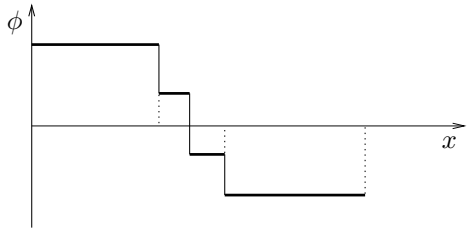

Figure 6. Cross section of initial level-set function for discretization P_1 in Figure 5. The level-set function is piecewise constant on each element.

function since we do not have enough information in the observation data to achieve fine-scale improvements on the zone geometry. The low number of parameters in the representation enables rapid localization of coarse-scale features of the permeability.

We start by defining the narrow band of cells that are allowed to change permeability values as the cells that are less than a certain number of grid cells away from the the zero isocontour. This gives us two bands corresponding to positive and negative values for ϕ^l. These bands are further divided into elements, each element corresponding to one parameter, a_s^l. We start off by a few elements of a given approximate length. As the optimization proceeds, we allow for more parameters by decreasing the approximate length of the elements.

There are usually several different ways the narrow band can be divided to achieve the desired approximate length of each element. The chosen strategy have influence on the result, but as long as the elements have roughly the same number of cells, it is not possible to determine a best strategy a priori. Since there are only minor and unsystematic differences in the results when following the different strategies, we do not go into details on our choice.

In the numerical examples in Section 6, we consider a uniform square grid with N_h grid cells in each direction, where the grid cells are of size $\Delta h \times \Delta h$. The support of each basis function χ_s^l cover approximately $N_p \times N_a$ grid cells as given in Table I. Here N_p denotes the number of grid cells counting in the direction perpendicular to the zero isocontour, N_a denotes the number of grid cells aligned with the

zero isocontour, and α equals x or y depending on the direction of the zero isocontour.

Table I. The number of grid cells covered by each basis function, χ_s^l, in the alternative discretizations P_1–P_5.

	P_1	P_2	P_3	P_4	P_5
N_p:	1	2	1	2	1
N_a:	N_α	$N_\alpha/2$	$N_\alpha/2$	$N_\alpha/4$	$N_\alpha/4$

5.4. Parameter Estimation Problem Revisited

The new level-set representation of the permeability allows us to alter the geometry of the zonation through changing signs of the parameters $\{a_s^l\}$, $s = 1, \ldots, N^l$, $a = 1, \ldots, n$. We do not optimize with respect to permeability values and the geometry of the zones simultaneously since difference in scaling can give instabilities in the procedure.

Holding $\mathbf{c}$ fixed, we can express the residual as a function of $\mathbf{a}$:

$$\mathbf{r}(\mathbf{a}) = \mathbf{d} - \mathbf{m}(\mathbf{a}).$$

For a given discretization of the level-set functions, the new parameter estimation problem with respect to $\mathbf{a}$ can be written as follows: Find $\mathbf{a}^*$ such that

$$\mathbf{a}^* = \arg\min_{\mathbf{a}} ||\mathbf{r}(\mathbf{a})||. \tag{5}$$

The objective function as a function of $\mathbf{a}$ is given as

$$f(\mathbf{a}) = (\mathbf{d} - \mathbf{m}(\mathbf{a}))^T \mathbf{D}^{-1} (\mathbf{d} - \mathbf{m}(\mathbf{a})), \tag{6}$$

where $\mathbf{D}$ as before is the covariance of the measurement errors. The problem is still a nonlinear weighted output least-squares problem, and we can apply the Levenberg-Marquardt algorithm. This optimization algorithm requires the matrix of sensitivities of model response with respect to model parameters.

5.5. Sensitivity Calculations

The sensitivity matrix is the derivative of model response $\mathbf{m}(\mathbf{c})$ or $\mathbf{m}(\mathbf{a})$ with respect to model parameters $\mathbf{c}$ or $\mathbf{a}$. The sensitivity matrix is an important component in the optimization procedure. Herein, we apply

a direct method for its computation (e.g., Tortorelli and Michaleris, 1994, Urkedal, 1998).

The direct method utilizes the solution of the forward problem to calculate the derivatives of the state variables with respect to the parameters of the model. With this method, a single run of the simulator calculates both the model output and the first order derivatives with respect to the parameters. Since more equations have to be solved at each time step, each run of the simulator requires more time. This is the most time consuming part of the optimization algorithm, also because the forward problem in itself requires heavy computations.

An alternative method is the adjoint state or optimal control method (Chen et al., 1974; Chavent et al., 1975). With this method, the solution of one adjoint system of equations is required for every gradient that is needed. This number is equal to one for the computation of the objective function gradient, and it is equal to the number of observations for the computation of the sensitivity matrix.

Which of the above methods that is more efficient in computing the sensitivity matrix depends on the number of observations compared to the number of parameters. In our case, where the number of parameters is significantly lower than the number of observations, the direct method is preferable.

Yet an alternative approach is the method of finite differences. For the derivative with respect to each parameter, this method requires multiple simulator runs. Hence, given our forward problem, the savings in computer time using the direct method are considerable even for a few parameters.

As the optimization with respect to $\mathbf{c}$ and $\mathbf{a}$ is separated in the numerical solution procedure, we need two different sensitivity matrices: one with respect to $\mathbf{c}$ and one with respect to $\mathbf{a}$. The sensitivity matrix with respect to each $\mathbf{a}^l$ component of $\mathbf{a}$ is

$$\mathbf{J}_{\mathbf{a}^l} = \begin{bmatrix} \frac{\partial m_1}{\partial a_1^l} & \frac{\partial m_1}{\partial a_2^l} & \cdots & \frac{\partial m_1}{\partial a_{N^l}^l} \\ \frac{\partial m_2}{\partial a_1^l} & \frac{\partial m_2}{\partial a_2^l} & \cdots & \frac{\partial m_2}{\partial a_{N^l}^l} \\ \vdots & \vdots & \ddots & \vdots \\ \frac{\partial m_M}{\partial a_1^l} & \frac{\partial m_M}{\partial a_2^l} & \cdots & \frac{\partial m_M}{\partial a_{N^l}^l} \end{bmatrix},$$

where the subscript on m denotes the index of the model output. Hence, $\frac{\partial m_r}{\partial a_s^l}$ is the sensitivity of the model pressure corresponding to the observation d_r with respect to the parameter a_s^l. By means of $\mathbf{J}_{\mathbf{a}^l}$, we can find how to change ϕ^l in all grid cells.

We choose to optimize with respect to all level-set functions simultaneously. The sensitivity matrix for the optimization with respect to

the vector $\mathbf{a}$ of all the coefficients for the level-set functions is then

$$\mathbf{J_a} = \left[\begin{array}{cccc} \mathbf{J}_{\mathbf{a}^1} & \mathbf{J}_{\mathbf{a}^2} & \cdots & \mathbf{J}_{\mathbf{a}^n} \end{array} \right].$$

In the same manner, the sensitivity matrix with respect to $\mathbf{c}$ is given by

$$\mathbf{J_c} = \begin{bmatrix} \frac{\partial m_1}{\partial c_1} & \frac{\partial m_1}{\partial c_2} & \cdots & \frac{\partial m_1}{\partial c_{2^n}} \\ \frac{\partial m_2}{\partial c_1} & \frac{\partial m_2}{\partial c_2} & \cdots & \frac{\partial m_2}{\partial c_{2^n}} \\ \vdots & \vdots & \ddots & \vdots \\ \frac{\partial m_M}{\partial c_1} & \frac{\partial m_M}{\partial c_2} & \cdots & \frac{\partial m_M}{\partial c_{2^n}} \end{bmatrix}.$$

Note that the dimension of $\mathbf{J_c}$ is $M \times 2^n$, while the dimension of $\mathbf{J}_{\mathbf{a}^l}$ is $M \times N^l$, and the dimension of $\mathbf{J_a}$ is $M \times \sum_{l=1}^{n} N^l$.

A step in obtaining the sensitivity matrices $\mathbf{J_a}$ and $\mathbf{J_c}$ is to estimate $\frac{\partial k}{\partial a_s^l}$ and $\frac{\partial k}{\partial c_i}$. In the general case of n level-set functions as given in equation (4), we see that

$$\frac{\partial k}{\partial c_i} = \prod_{j=1}^{n} R_i(\phi^j),$$

and

$$\frac{\partial k}{\partial \phi^l} = \sum_{i=1}^{2^n} c_i \left(\prod_{j=1, j\neq l}^{n} R_i(\phi^j) \right) D_i(\phi^l), \tag{7}$$

where

$$D_i(\phi^l) = \frac{dR_i}{d\phi^l} = \begin{cases} \delta(\phi^l), & \text{if } b_l^i = 0, \\ -\delta(\phi^l), & \text{if } b_l^i = 1. \end{cases}$$

In the above, δ denotes the Dirac delta function. It can be seen that $\frac{\partial k}{\partial c_i}$ is nonzero only in the region corresponding to $k = c_i$. Inside this region, $\frac{\partial k}{\partial c_i} = 1$.

For $\frac{\partial k}{\partial a_s^l}$, we obtain

$$\frac{\partial k}{\partial a_s^l} = \frac{\partial k}{\partial \phi^l} \frac{\partial \phi^l}{\partial a_s^l} = \sum_{i=1}^{2^n} c_i \left(\prod_{j=1, j\neq l}^{n} R_i(\phi^j) \right) D_i(\phi^l) \chi_s^l,$$

where we have inserted the expression for $\frac{\partial k}{\partial \phi^l}$ given in equation (7).

For computational reasons, the δ function is replaced by δ_ϵ, where δ_ϵ is a smoothed counterpart. We have applied the following function (Vese and Chan, 2002; Chan and Tai, 2003):

$$\delta_\epsilon(\phi) = \frac{\epsilon}{\pi(\phi^2 + \epsilon^2)}.$$

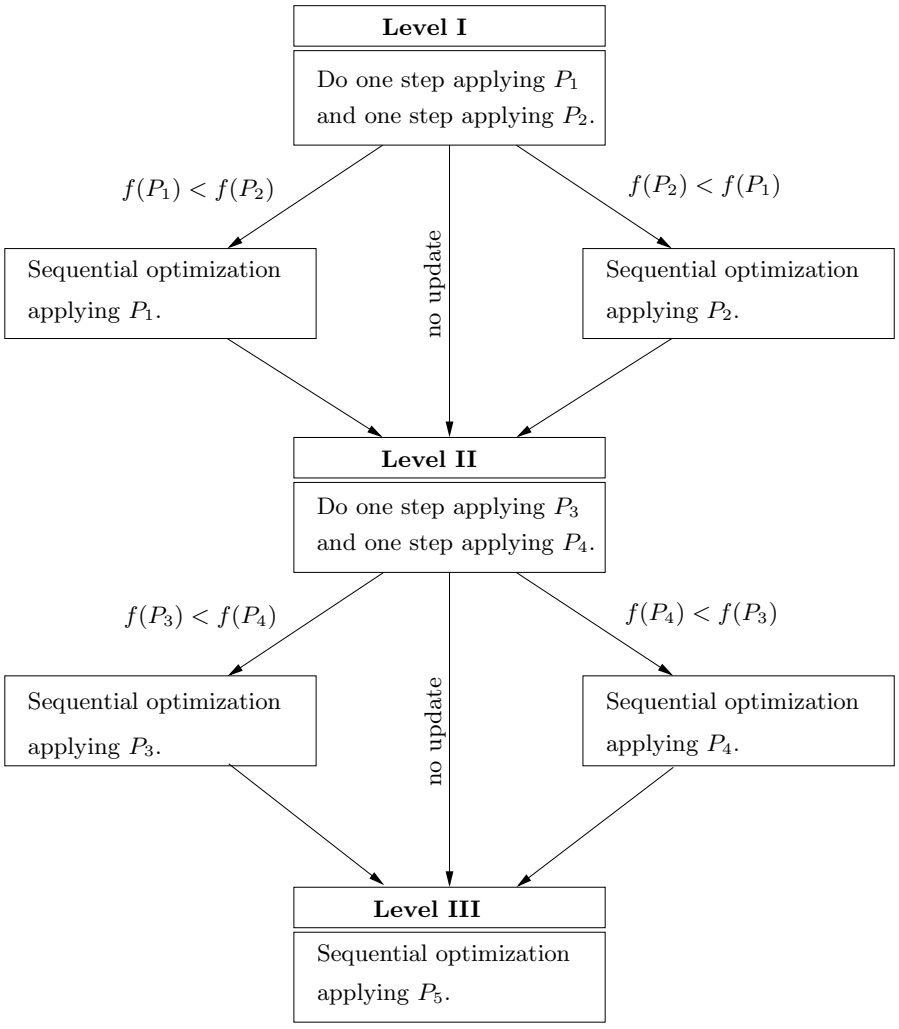

Figure 7. Choice of parameterization at different levels in the estimation procedure.

For our test cases, we found that taking $\epsilon = \Delta h$ was a good choice; see also Chan and Tai (2003).

5.6. Algorithm

We are now ready to present the numerical algorithm for the parameter estimation problem.

To solve the optimization problems, we use the Levenberg-Marquardt method (e.g., Moré, 1977, Nocedal and Wright, 1999).

We apply a sequential estimation procedure where we alternate between optimization with respect to $\mathbf{c}$ and $\mathbf{a}$. Every step of $\mathbf{a}$-optimization that results in an update in the geometry of the zones is followed by *two* steps of $\mathbf{c}$-optimization. The reason we apply the proportion, $1:2$, between $\mathbf{a}$- and $\mathbf{c}$-optimization, is that one update of $\mathbf{a}$ affects the permeability distribution more strongly than a step of $\mathbf{c}$-optimization.

The algorithm has three levels, where each level corresponds to one choice of discretization for the level-set functions. The different levels in the optimization procedure are illustrated in Figure 7.

Based on the result of AME, we start off by comparing the objective-function values after one step of $\mathbf{a}$-optimization with discretizations P_1 and P_2 at Level I. If neither of the discretizations P_1 or P_2 results in any updates on the geometry, we move on to Level II. Otherwise the discretization giving the least objective-function value is chosen. In the latter case, we continue by doing optimization with respect to $\mathbf{c}$. We continue sequentially, alternating between optimization with respect to $\mathbf{a}$ and $\mathbf{c}$, until $\mathbf{a}$-optimization fails to give any updates in the geometry of the zones. At this point we go to the next level.

At Level II, we repeat the procedure from Level I, except that now we compare discretizations P_3 and P_4.

At Level III in the optimization procedure, we continue the sequential optimization with discretization P_5.

An unfortunate discretization can give results that lead the optimization onto a wrong track. Discretizations P_1 and P_2 are qualitatively different. The ability to choose between them initially, makes the algorithm more flexible for handling of different permeability structures with a minimum number of elements. The same argument applies for discretizations P_3 and P_4.

The algorithm below describes the estimation procedure for each level of discretization.

ALGORITHM 5.1. *Start at Level I. Set k=0. Choose initial* $\mathbf{a}^0$ *and* $\mathbf{c}^0$*. While the solution criterion is not reached:*

1. *If we are at the start of Level I or Level II, do step 2 for both discretizations. Choose the discretization strategy that gave the least residual at the current level.*

2. *Initialize* $\{\phi^{l,k}\}$, $l = 1, \ldots, n$ *to be approximations to signed distance functions on the current discretization grid. Update* $\mathbf{a}^k$*:*

$$\mathbf{p_a} = \arg\min_p ||\mathbf{J}^k_{\mathbf{a}}\mathbf{p} + \mathbf{r}_k||_2^2 \qquad \textit{for } ||\mathbf{p}|| < \Delta^k_{\mathbf{a}},$$
$$\mathbf{a}^{k+1} = \mathbf{a}^k + \mathbf{p}^k_{\mathbf{a}}$$

3. *If an update in the geometry of zones was found for the current parameterization go to step 4. Else if at Level III stop. Else shift to next level and go to 1.*

4. *Update* $\mathbf{c}$*:*

$$\mathbf{p_c} = \arg\min_{\mathbf{p}} ||\mathbf{J}_{\mathbf{c}}^k \mathbf{p} + \mathbf{r}_k||_2^2 \qquad \textit{for } ||\mathbf{p}|| < \Delta_{\mathbf{c}}^k,$$
$$\mathbf{c}^{k'} = \mathbf{c}^k + \mathbf{p}_{\mathbf{c}}^k$$
$$\mathbf{c}^{k+1} = \mathbf{c}^{k'} + \mathbf{p}_{\mathbf{c}}^{k'}$$

5. *Let* $k = k + 1$ *and go to 2.*

Here $\Delta_{\mathbf{a}}^k$ and $\Delta_{\mathbf{c}}^k$ are the respective trust-region radiuses.

The focus in this work is on the potential of the LSC approach. In many of the numerical examples in Section 6, we therefore demonstrate optimization with respect to $\mathbf{a}$ only.

Since we do a trust-region search in the optimization algorithm, it is desirable to control the magnitude of the parameters. Hence, we reinitialize the level-set functions as approximations to signed distance functions at the start of each step. Recall, however, that it is only the sign of the level-set functions that has influence on the resulting permeability representation.

5.7. Initial Guess for Permeability

An initial guess for the level-set representation of $k(\mathbf{x})$ is obtained according to an expected result from AME,

$$k(\mathbf{x}) = \sum_{i=1}^{Z} c_i^{AME} \psi_i^{AME}(\mathbf{x}),$$

where $\{\psi_i^{AME}(\mathbf{x})\}$ denotes a set of characteristic basis functions. For each value of the permeability, we define a region, and take

$$c_i^0 = c_i^{AME}, \qquad \prod_{j=1}^{n} R_i(\phi^j) = \psi_i^{AME}, \qquad i = 1, \ldots, Z,$$

if there are Z distinct permeability values. In this case, the number of level-set functions is

$$n = \text{ceil}\Big(\log_2(Z)\Big),$$

where ceil rounds $\log_2(Z)$ up to the nearest integer. If the number of distinct permeability values, Z, is less than the number of regions

defined by the level-set functions, 2^n, we require that $c_i = c_{i-1},\ i = Z+1,\ldots,2^n$, and divide region Z into $2^n - Z + 1$ pieces defining a new R_i for each c_i, where $i = Z,\ldots,2^n$. In other words, some zones are associated with the same zonal value.

6. Numerical Results

In this section, we present various examples to study the performance of the level-set approach. We apply a reasonable initial permeability guess for the LSC procedure according to what could be expected from AME as predictor. The results are obtained with a realistic, sparse data density.

In Table II, we list the physical characteristics of the model reservoir. The dimensions of the square, horizontal reservoir are given as L for the horizontal extent and h for the thickness. All specifications are presented dimensionless. The pressure, $p = p_o = p_w$ ($P_c \equiv 0$), is logged in the injection wells during production. In Table III, details of the measurements are given.

Table II. Fixed reservoir and fluid properties

Reservoir dimensions	$L = 1.0$	$h = 6.25 \cdot 10^{-2}$
Initial saturation	$S_w = 0.1$	$S_o = 0.9$
Viscosities	$\mu_w = 1.0$	$\mu_o = 1.3$
Porosity	$\varphi = 0.3$	
Relative permeability function	$k_{rw}(S_w) = \frac{(S_w-0.1)^2}{(1-0.8)^2}$	$k_{ro}(S_w) = \frac{(0.8-S_w)^2}{(1-0.8)^2}$
Capillary pressure	$P_c(s_w) \equiv 0$	

Table III. Details of measurements

Number of observations for each injector	$n = 200$
Observation times	$t = i\Delta t,\ \Delta t = 0.005,\ i = 1,\ldots,n$
St.deviation of measurement errors	$\sigma_I = 1.55 \cdot 10^1,\ \sigma_{II} = 1.55 \cdot 10^2$
Total injection rate	$7.81 \cdot 10^{-3}$

To obtain observation data $\mathbf{d}^M$ of the pressure, we added measurement errors to the pressure values obtained from a run of the simulator with the reference permeability field. The measurement errors are normally distributed. For all subsequent examples, we consider two test cases with different level of measurement error. In Case I, the

standard deviation is σ_I on the measurement errors, while for Case II, the standard deviation is σ_{II}. For the numerical examples we have investigated, the standard deviations σ_I and σ_{II} correspond to about 0.1% and 1% of the maximum pressure difference between the injectors and producer during the simulated time period.

All the forward flow simulations are done on a 16×16 grid. The wells are positioned in the corners: one production and three injection wells. These are shown as white dots in the figures. The injection rate is set to $3.91 \cdot 10^{-3}$ in the injector diagonally from the producer. In the two other injectors, the injection rate is set to $1.95 \cdot 10^{-3}$. The pressure in the producer is constant.

For all the examples, a table giving the the initial objective-function value, f^i, the limit in the solution criterion (2), f^{sc}, and the objective-function value at the end of the estimation, f^f, is provided. We also specify the number of updates for the chosen discretizations.

We remark that the non-integer values of the reference permeabilities are due to the scaling of the reservoir into dimensionless form.

6.1. Optimization with Respect to Shape of Zones; Correct Zonal Values

We first give examples where we optimize with respect to the geometry of the zones through optimizing the parameters $\{\mathbf{a}^l\}$, $l = 1, \ldots, n$, for different discretizations for the level-set functions. The constant permeability values, $\mathbf{c}$, are kept fixed. In all cases, the initial permeability guess has correct constant permeability values, $\mathbf{c}$, but incorrect geometry of the zones.

EXAMPLE 1. In the current estimation, we seek to reproduce a permeability field of two distinct values, where the geometry of the zones is described by one level-set function. The production well is placed in the lower right corner, while the injection wells are located in the remaining corners.

Results are shown in Figure 8. Figure 9 shows the updates of the permeability for each applied discretization. Details of the estimation are provided in Table IV.

For this example, it is impossible to completely recover the reference permeability field since we apply only discretizations P_1–P_5 described in Section 5.6. For this test, there is no obvious best discretization strategy for the level-set functions at the first steps.

Table IV. Details of the estimation for Example 1 in Cases I and II.

	f^i	f^{sc}	f^f	geometry updates
Case I	$3.44 \cdot 10^6$	$6.22 \cdot 10^2$	$1.42 \cdot 10^4$	$1\times P_1,\ 2\times P_4,\ 1\times P_5$
Case II	$3.49 \cdot 10^4$	$6.20 \cdot 10^2$	$7.52 \cdot 10^2$	$1\times P_1,\ 2\times P_4,\ 4\times P_5$

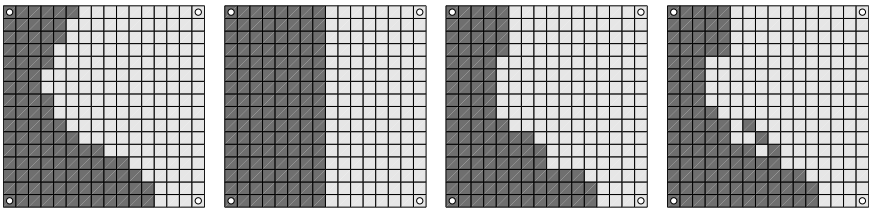

Figure 8. From left to right: Reference permeability, initial permeability, and final estimate for Cases I and II. The permeability values are 1.95 in the left region and 5.86 in the right region.

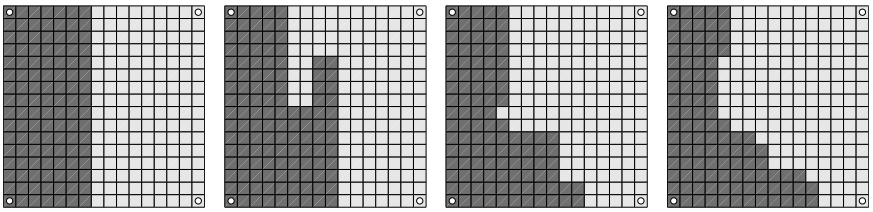

Figure 9. From left to right: Sequential geometry updates for Case I until final estimate.

Despite an equal initial permeability guess, f^i corresponding to Case II is greater than f^i of Case I. The reason is the objective function being scaled by the inverse of the covariance matrix; see Equation (1). This reflects that if the noise level is high, the data foundation is weak with respect to improvements in the permeability estimation giving a low objective function value. The performance of the estimation algorithm is, therefore, best reflected in the relative reduction of f.

EXAMPLE 2. We seek to reproduce a permeability field of three distinct values, where the geometry of the zones is described by two level-set functions. The production well is placed in the upper left corner, while the injection wells are located in the remaining corners.

Figure 10 shows the reference and initial permeability fields together with the final estimates. Details of the estimation are provided in Table V.

Table V. Details of estimation for Example 2 in Cases I and II.

	f^i	f^{sc}	f^f	geometry updates
Case I	$1.03 \cdot 10^7$	$6.10 \cdot 10^2$	$1.81 \cdot 10^3$	$2\times P_2$, $3\times P_5$
Case II	$1.02 \cdot 10^5$	$6.05 \cdot 10^2$	$1.02 \cdot 10^3$	$2\times P_2$, $4\times P_5$

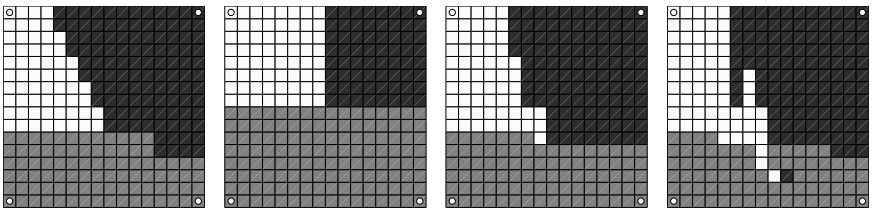

Figure 10. From left to right: Reference permeability, initial permeability, and final estimate for Cases I and II. The permeability values are 9.77 and 1.17 in the left and right upper regions and 3.12 in the bottom region.

EXAMPLE 3. In the current example, we look at a permeability field consisting of four zones of different constant permeability values. The production well is placed in the upper right corner, while the injection wells are located in the remaining corners. For both Case I and Case II, the reference permeability field was recovered, see Figure 11. Details of the estimation are provided in Table VI.

Table VI. Details of estimation for Example 3 in Cases I and II.

	f^i	f^{sc}	f^f	geometry updates
Case I	$1.49 \cdot 10^7$	$6.24 \cdot 10^2$	$5.88 \cdot 10^2$	$2\times P_1$
Case II	$1.50 \cdot 10^5$	$6.24 \cdot 10^2$	$6.17 \cdot 10^2$	$2\times P_1$

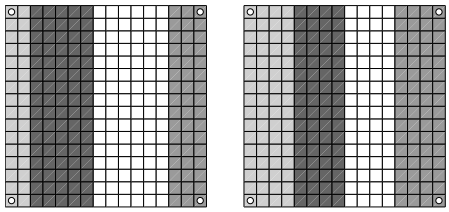

Figure 11. Reference and recovered permeability (left), initial permeability (right). The permeability values are, respectively, 3.91, 0.98, 7.81, 1.95, from the left to the right region.

EXAMPLE 4. We consider the same setup as in the previous example, but with different reference and initial distribution of the permeability. Figure 12 shows the reference and initial permeability field together with the final estimates. Details of the estimation are provided in Table VII.

Table VII. Details of estimation for Example 4 in Case I and II.

	f^i	f^{sc}	f^f	geometry updates
Case I	$3.44 \cdot 10^7$	$6.14 \cdot 10^2$	$4.34 \cdot 10^4$	$2\times P_2,\ 1\times P_3,\ 1\times P_5$
Case II	$3.44 \cdot 10^5$	$6.14 \cdot 10^2$	$7.95 \cdot 10^2$	$2\times P_2,\ 4\times P_5$

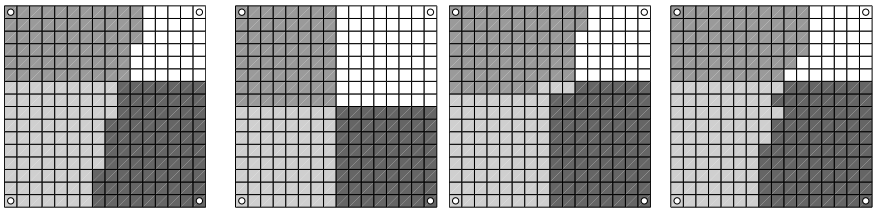

Figure 12. From left to right: Reference permeability, initial permeability, and final estimate for Cases I and II. The permeability is, respectively, 1.95, 7.81, 0.98 and 3.91, counting clockwise from the upper left region.

6.2. Optimization with Respect to Shape of zones and Zonal Values

Now we give examples where we optimize both with respect to the shape of the zones, defined by $\mathbf{a}$, and the different permeability values,

$\mathbf{c}$, inside the zones. In these examples, the initial permeability guess has both incorrect permeability values and incorrect zone geometry.

In the subsequent examples, we have used the following additional notation: $\mathbf{c}^i$ denotes the initial permeability values, $\mathbf{c}^r$ is the vector of reference permeability values and $\mathbf{c}^f$ is the final permeability estimate.

EXAMPLE 5. In this example, we seek to recover a reference permeability distribution of two distinct values. The initial permeability values differ by 10% from the reference permeability values, so that the initial field has a stronger permeability contrast than the reference field. The production well is placed in the lower right corner, while the injection wells are located in the remaining corners.

Table VIII. Details of estimation for Example 5 in Case I and II.

	f^i	f^{sc}	f^f	geometry updates
Case I	$8.58 \cdot 10^7$	$6.24 \cdot 10^2$	$6.90 \cdot 10^4$	$2\times P_2$, $1\times P_4$, $1\times P_5$
Case II	$8.59 \cdot 10^5$	$6.24 \cdot 10^2$	$1.46 \cdot 10^3$	$2\times P_2$, $2\times P_5$
	$\mathbf{c}^i$	$\mathbf{c}^r$	$\mathbf{c}^f$	
Case I	[6.45, 1.76]	[5.86, 1.95]	[5.84, 1.94]	
Case II	[6.45, 1.76]	[5.86, 1.95]	[5.75, 1.94]	

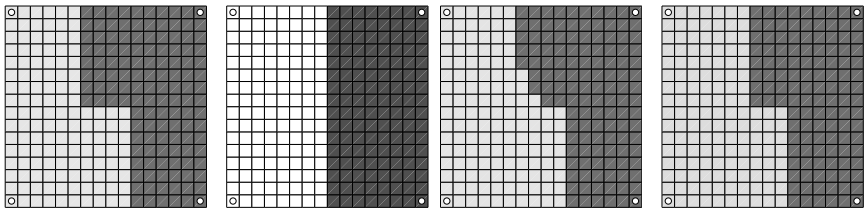

Figure 13. From left to right: Reference permeability, initial permeability, and final estimate for Case I and Case II. The permeability values are 5.86 in the left region and 1.95 in the right region for the reference permeability field, whereas the initial permeability field is 6.45 in the left region and 1.76 in the right region.

Figure 13 shows the reference and initial permeability field together with the final estimates. We approach both the reference permeability values and the reference geometry. Details of the estimation are provided in Table VIII.

EXAMPLE 6. We consider the same setup as in Example 5. As in Example 5, the initial permeability values differ by 10% from the reference permeability values, but now the permeability contrast is lower for the initial than for the reference permeability distribution.

Figure 14 shows the reference and initial permeability field together with the final estimates. We see that both the final permeability values and zone geometry differ from the reference permeability even though the results are a significant improvement on the initial guess. Details of the estimation are provided in Table IX.

Table IX. Details of estimation for Example 6 in Case I and II.

	f^i	f^{sc}	f^f	geometry updates
Case I	$1.61 \cdot 10^7$	$6.20 \cdot 10^2$	$7.12 \cdot 10^5$	$2\times P_2$, $1\times P_3$
Case II	$1.61 \cdot 10^5$	$6.24 \cdot 10^2$	$8.97 \cdot 10^3$	$2\times P_2$
	$\mathbf{c}^i$	$\mathbf{c}^r$	$\mathbf{c}^f$	
Case I	$[5.27, 2.15]$	$[5.86, 1.95]$	$[7.23, 2.03]$	
Case II	$[5.27, 2.15]$	$[5.86, 1.95]$	$[7.24, 2.03]$	

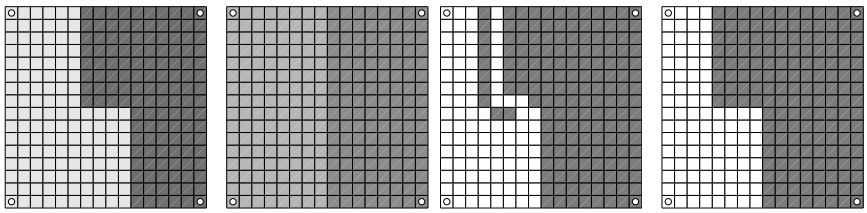

Figure 14. From left to right: Reference permeability, initial permeability, and final estimate for Case I and Case II. The permeability values are 5.86 in the left region and 1.95 in the right region for the reference permeability field, whereas the initial permeability field is given by 5.27 in the left region and 2.15 in the right region.

EXAMPLE 7. For this last example, we look at how small perturbations on the reference coarse-scale permeability field from Examples 5 and 6 affect the ability to reconstruct the main permeability shifts. The small perturbations are random and normally distributed with standard deviation $\sigma = 0.17$.

Figure 15 shows the reference and initial permeability fields together with the final estimates. Given the two different noise levels, the resulting geometries are equal.

The coarse-scale permeability shift is recovered applying only a low number of level-set parameters (P_2). As the number of parameters

increases (P_5), the fine-scale permeability perturbations have a stronger influence on the resulting parameter estimates. This results in a small deviation on the coarse-scale permeability shift.

Details of the estimation are provided in Table X.

Table X. Details of estimation for Example 7 in Case I and II.

	f^i	f^{sc}	f^f	geometry updates
Case I	$7.66 \cdot 10^6$	$6.24 \cdot 10^2$	$5.43 \cdot 10^4$	$1\times P_2$, $1\times P_5$
Case II	$7.57 \cdot 10^5$	$6.24 \cdot 10^2$	$9.59 \cdot 10^2$	$1\times P_2$, $1\times P_5$
	$\mathbf{c}^i$	$\mathbf{c}^f$		
Case I	[5.86, 1.95]	[5.77, 1.97]		
Case II	[5.86, 1.95]	[5.79, 1.97]		

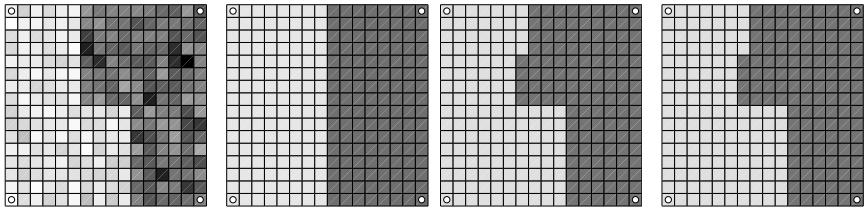

Figure 15. From left to right: Reference permeability, initial permeability and final estimate for Case I and Case II. The reference permeability field is obtained by adding random perturbations with a standard deviation of $\sigma = 0.17$ to a permeability field of 5.86 in the left region and 1.95 in the right region. The initial permeability field is given by 5.86 in the left region and 1.95 in the right region.

6.3. Summary of Results

The examples show that the level-set corrector provides significant reduction in the objective-function values. We observe a considerable improvement in the geometry of the zones, although the solution criterion is not reached for most of the test examples. One reason for this are the coarse discretizations for the level-set functions. This choice of not looking for finer-scale features of the permeability is related to our wish of combining the level-set strategy with AME in a complete, sequential predictor-corrector approach.

The estimations are stable with respect to the different noise levels in the observation data. Since the variance error in the estimation increases with the number of parameters, the level-set corrector is more

stable with respect to noise at the start of the estimation when a coarse discretization is applied.

For the examples in Section 6.2, where the initial permeability values deviate from the reference values, it becomes more difficult to recover the reference geometry of the zones. In this case, the updates of the permeability values can compensate for erroneous geometry. This is most profound in Example 6.

7. Remarks on How to Further Combine AME and LSC

For future work, other aspects also arise in order to combine AME and LSC. How early in the process of AME is it best to correct the result by the level-set approach, and how far should the correction be driven before it is better to do the next step of AME, dividing the reservoir into finer sub-regions?

Based on the results so far, we recommend the introduction of the corrector step at an early stage in order to correct erroneous geometry from AME and, hence, control the number of parameters. However, at an early stage of AME the number of sub-regions may be too low to reproduce the coarse-scale structures of the true permeability distribution. The objective for the correcting step would then not be to solve the inverse problem, but rather to make a significant reduction of the objective function based on the given number of regions. A measure of the attainable objective function value corresponding to a given number of parameters would then have to be developed, for example, inspired by the approach of Grimstad et al. (2003).

Remark. A paper proposing a methodology for a full combination of LSC and AME, expanding on the ideas of this paper and submitted after it, has already been published; see Lien et al. (2006).

8. Conclusions

Parameterization of the permeability by level-set functions provides an opportunity to change boundaries between zones of constant permeability value. This enables an adaptive adjustment of boundaries into fairly general geometries.

In combination with adaptive multiscale estimation, the level-set representation of permeability has the potential of recovering the coarse-scale permeability structures with a rather low number of parameters.

Numerical examples show that the introduction of the level-set corrector after adaptive multiscale prediction improves the permeability estimates significantly.

Acknowledgements

Two of the authors (Martha Lien and Trond Mannseth) have been supported by a research program within inverse problems, financed by ENI SpA, Norsk Hydro ASA and the Norwegian Research Council (Grant no.: 146528/210). This support is gratefully acknowledged.

References

D. Adalsteinsson and J. A. Sethian. A fast level set method for propagating interfaces. *J. Comput. Phys.*, 118(2):269–277, 1995.

M. Burger. Levenberg-Marquardt level set methods for inverse obstacle problems. *Inverse Problems*, 20:259–282, 2004

H. Ben Ameur, G. Chavent and J. Jaffré. Refinement and coarsening indicators for adaptive parameterization: application to the estimation of hydraulic transmissivities. *Inverse Problems*, 18(3):775–794, 2002.

T. Chan and X.-C. Tai. Level set and total variation regularization for elliptic inverse problems with discontinuous coefficients. *J. Comput. Physics*, 193:40–66, 2003.

J. Carrera. State of the art of the inverse problem applied to the flow and solute transport equation. In E. Custiodio, A. Gurgui, and J. P. Lobo Ferreira, editors, *Proc. of the NATO Advanced Workshop on Advances in Analytical and Numerical Groundwater Flow and Quality Modelling (Lisbon, Portugal, June 2-6, 1987)*, volume 224 of *NATO ASI Series, Series C: Mathematical and Physical Sciences*, pages 549–583, Dordrecht, Holland, 1988. D. Reidel Publishing Company.

G. M. Chavent, M. Dupuy, and P. Lemonnier. History matching by use of optimal control. *SPE Journal*, 15(1):74–86, February 1975.

W. H. Chen, G. R. Gavalas, J. H. Seinfeld, and M. L. Wasserman. A new algorithm for automatic history matching. *SPE Journal*, 14(6):593–608, December 1974.

Y. Emsellem and G. de Marsily. An automatic solution for the inverse problem. *Water Resour. Res.*, 7, pages 1264–1283, 1971.

G. R. Gavalas, P. C. Shah, and J. H. Seinfeld. Reservoir history matching by Bayesian estimation. In *SPE-AIME Fourth Symposium on Numerical Simulation or Reservoir Performance (Los Angeles)*, SPE 5740. Society of Petroleum Engineers, 1976.

A.-A. Grimstad, T. Mannseth, G. Nævdal, and H. Urkedal. Adaptive multiscale permeability estimation. *Comput. Geosci.*, 7(1):1–25, 2003.

B.-O. Heimsund, T. Chan, T.K. Nilssen and X.-C. Tai. Level set methods for a parameter identification problem. Analysis and optimization of differential systems (Constanta, 2002),189–200, Kluwer Acad. Publ., Boston, MA, 2003.

M. Hintermüller and W. Ring An inexact Newton-CG-type active contour approach for the minimization of the Mumford-Shah functional. *J. Math. Imag.Vision*, 2003, to appear.

K. Ito, K. Kunisch and Z. Li. Level-set function approach to an inverse interface problem. *Inverse Problems*, 17(5):1225–1242, 2001.

P. Jacquard. Théorie de l'interprétation des mesures de pression. *Revue IFP*, XIX, March 1964.

P. Jacquard and C. Jain. Permeability distribution from field pressure data. *SPE Journal*, December 1965.

A. Kirsch. *An introduction to the theory of inverse problems*, volume 120 of *Applied mathematical sciences*. Springer-Verlag, New York, 1996.

H. Krüger and T. Mannseth. Extension of the parameterization choices in adaptive multiscale permeability estimation. Accepted for publication in *Inverse problems in Science and Engineering*.

G. de Marsily. Spatial variability of properties in porous media: A stochastic approach. In J. Bear and M. Y. Corapcioglu, editors, *Fundamentals of Transport in Porous Media*, pages 719–769. Martinus Nijhoff, Boston, 1984.

G. de Marsily, J. P. Delhomme, A. Coudrain-Ribstein, and A. M. Lavenue. Four decades of inverse problems in hydrogeology. In D. Zhang and C. L. Winter, editors, *Theory, Modeling, and Field Investigation in Hydrogeology: A Special Volume in Honor of Shlomo P. Neuman's 60th Birthday*, Special Paper 348, pages 1–17. Geological Society of America, 2000.

M. Lien, I. Berre, and T. Mannseth. Combined Adaptive Multiscale and level-set parameter estimation. *Multiscale Modeling and Simulation*, 4(4):1349–1372, 2006.

D. McLaughlin and L. R. Townley. A reassessment of the groundwater inverse problem. *Water Resour. Res.*, 1996.

J. J. Moré The Levenberg-Marquardt algorithm: Implementation and theory. *Numerical Analysis, Lecture Notes in Mathematics*, vol. 630, pages 105–116. Springer Verlag, Berlin, 1977.

J. Nocedal and S. J. Wright. *Numerical Optimization*. Springer, 1999.

D. S. Oliver, A. C Reynolds, Z. Bi, and Y. Abacioglu. Integration of production data into reservoir models. *Petroleum Geoscience*, 7:65–73, 2001.

S. Osher and R. Fedkiw. *Level Set Methods and Dynamic Implicit Functions*. Springer, 2003.

S. Osher and J. A. Sethian. Fronts propagating with curvature-dependent speed: algorithms based on Hamilton-Jacobi formulations. *J. Comput. Phys.*, 79(1):12–49, 1988.

D. Peng, B. Merriman, S. Osher, H. Zhao, and M. Kang. A pde based fast local level set method. *Journal of Computational Physics*, 155:410–38, 1999.

F. Santosa A level-set approach for inverse problems involving obstacles *ESAIM Contrôle Optim. Calc. Var.*, 1:17–33 (electronic), 1995/96.

A. Sen and M. Srivastava. *Regression Analysis; Theory, Methods and Applications*. Springer-Verlag, 1990.

N.-Z. Sun. *Inverse problems in groundwater modeling*. Kluwer academic publishers, Dordrecht, 1994.

X.-C. Tai and T. F. Chan. Multiple level set methods and some applications for identifying piecewise constant functions.

D. A. Tortorelli and P. Micaleris. "Design Sensitivity Analysis: Overview and Review", *Inverse Problems in Engineering*, 1(1):71–105, 1994.

H. Urkedal. *Design of Multiphase Flow Equations*. PhD thesis, Department of Physics, University of Bergen, 1998.

L. A. Vese and T. F. Chan. A Multiphase Level Set Framework for Image Segmentation Using the Mumford and Shah Model. *International Journal of Computer Vision*, 50(3): 271–293, 2002.

W. W.-G Yeh. Review of parameter identification procedures in groundwater hydrology: The inverse problem. *Water Resour. Res.*, 22(2):95–108, 1986.

S. Yoon, A.H. Malallah, A. Datta-Gupta, D. W. Vasca and R. A. Beherens A multiscale approach to production data using streamline models. In *1999 SPE Annual Technical Conference and Exhibition. Society of Petroleum Engineers, October 1999. SPE 56653.*